

Multiferroicity in Ga-substituted LuFeO₃: A first-principles study

Xin Wang^{1,2,3}, Yehui Zhang,¹ Shiji Xu,¹ Xiang Ming Chen^{4,*}, Laurent Bellaiche,³ and Bin Xu^{1,†}

¹*Institute of Theoretical and Applied Physics, Jiangsu Key Laboratory of Thin Films, School of Physical Science and Technology, Soochow University, Suzhou 215006, China*

²*School of Sciences, Nantong University, Nantong 226019, China*

³*Physics Department and Institute for Nanoscience and Engineering, University of Arkansas, Fayetteville, Arkansas 72701, USA*

⁴*Laboratory of Dielectric Materials School of Materials Science and Engineering, Zhejiang University, Hangzhou 310027, China*



(Received 4 November 2022; revised 7 October 2023; accepted 18 October 2023; published 16 November 2023)

We report a theoretical design of multiferroic Lu_{1-x}Ga_xFeO₃ based on density functional theory calculations. While bulk LuFeO₃ stabilizes in a nonpolar *Pnma* structure, varying the concentration of Ga inside Lu_{1-x}Ga_xFeO₃ is predicted to result in the following structural transitions: *Pnma* ($x = 0 - 0.29$) → *P6₃cm* ($x = 0.29 - 0.81$) → *Pna2₁* ($x = 0.81 - 1$). The hexagonal *P6₃cm* phase possesses both a finite polarization and weak ferromagnetic moment, while the *Pna2₁* phase is ferroelectric and antiferromagnetic. Moreover, noncollinear magnetism (associated with spin-orbit coupling) is found to be critical for the stabilization of this *P6₃cm* phase. Variation of the electronic properties, such as density of states and band gap, are also reported.

DOI: [10.1103/PhysRevMaterials.7.114406](https://doi.org/10.1103/PhysRevMaterials.7.114406)

I. INTRODUCTION

Multiferroic materials exhibiting both ferroelectric and magnetic orders are not only promising for designing novel spintronic devices but are also of fundamental interest [1–3]. To date, hexagonal LuFeO₃ (*h*-LuFeO₃, space group *P6₃cm*) has gained much attention due to its room-temperature multiferroic properties [2,4–6]. In *h*-LuFeO₃, the inversion symmetry is broken due to the tilts of FeO₅ trigonal bipyramids, giving rise to ferroelectricity with a polarization value around 10 μC/cm² and with a high Curie temperature of 1050 K [2,6–9]. Moreover, *h*-LuFeO₃ film has an antiferromagnetic (AFM) order with a Néel temperature of 440 K [6]. Interestingly, for temperatures below 130 K, the magnetic moments carried by Fe ions are mostly aligned in the *a*-*b* plane in a 120° antiferromagnetic order, but with an additional small canting of the spins in the out-of-plane direction leading to a weak magnetization [6,10–12]. However, preparation of high-quality single-phase *h*-LuFeO₃ (*P6₃cm*) is challenging due to its metastable nature, i.e., the synthesis of LuFeO₃ often results in the nonpolar orthorhombic *Pnma* perovskite phase or a mixture of the two phases [13,14].

Various efforts have been devoted to stabilize the multiferroic *h*-LuFeO₃ phase. For instance, *h*-LuFeO₃ in a thin-film form can be stable under epitaxial strain [6,12,15]. Doping is also found to be effective for such stabilization with, e.g., Mn doping at the Fe site or Sc doping at the Lu site [16]. Specifically, the hexagonal state of Lu_{1-x}Sc_xFeO₃ is stabilized when the composition *x* is between 0.4 and 0.6 [16,17], and multiferroicity with noncollinear magnetic order and ferroelectricity was predicted based on first-principles

calculations [18]. In addition, the *P6₃cm* phase can also be realized experimentally in Lu_{1-x}In_xFeO₃ ($x = 0.4 - 0.6$) ceramics [19]. Therefore, a rule of thumb for creating the hexagonal phase with *A*-site substitution is to introduce chemical pressure with a trivalent element of a smaller ionic radius than Lu³⁺ (0.861 Å with a coordination of 6); for example, the radii of Sc³⁺ and In³⁺ are 0.745 and 0.8 Å, respectively. Sc is the smallest IIIB-group element, while, for the IIIA group, there are elements smaller than In, such as Ga that has an ionic radius of 0.62 Å. On the other hand, note that GaFeO₃ has an orthorhombic ground state of *Pna2₁* space group, which can also be regarded as multiferroic in a broader sense, as it exhibits both antiferromagnetic (AFM) and ferroelectric orderings [20–22]. It is therefore interesting to check if Lu_{1-x}Ga_xFeO₃ can be stabilized in the *P6₃cm* phase with intermediate compositions in between the *Pnma* phase of pure LuFeO₃ and the *Pna2₁* phase of pure GaFeO₃, and to also check if it can be multiferroic.

In this paper, we aim to explore structural phase transitions and multiferroic properties in Lu_{1-x}Ga_xFeO₃ with *x* ranging from 0 to 1 via first-principles simulations. We predict that bulk Lu_{1-x}Ga_xFeO₃ undergoes a *Pnma* ($x = 0 - 0.29$) → *P6₃cm* ($x = 0.29 - 0.81$) → *Pna2₁* ($x = 0.81 - 1$) structural phase sequence, with noncollinear magnetism arising from spin-orbit coupling (SOC) being crucial for that sequence. Also, both the polarization and magnetism are affected by varying the concentration of Ga, and the ferroelectric polarization of Lu_{1-x}Ga_xFeO₃ ($x = 0.92$) in the *Pna2₁* phase can be slightly enhanced to 29 μC/cm² with respect to that of the *P6₃cm* phase (about 17 μC/cm²). The electronic properties of Lu_{1-x}Ga_xFeO₃ are also investigated.

This paper is organized as follows. Section II provides details about the computational methods. In Sec. III, the crystal and magnetic structures of the *Pnma*, *P6₃cm*, and *Pna2₁* phases are presented, followed by the prediction of

*xmchen59@zju.edu.cn

†binxu19@suda.edu.cn

the structural evolution in $\text{Lu}_{1-x}\text{Ga}_x\text{FeO}_3$ with increasing Ga composition, and the multiferroic and electronic properties of $\text{Lu}_{1-x}\text{Ga}_x\text{FeO}_3$ are also reported. Finally, Sec. IV summarizes the main findings.

II. COMPUTATIONAL METHOD

Density functional theory (DFT) calculations were carried out using the Vienna *ab initio* simulation package (VASP) [23,24]. A plane-wave basis set with an energy cutoff of 500 eV was used with the projector augmented wave (PAW) method to mimic electron-ion interactions [24]. Generalized gradient approximation plus U (GGA + U) with Perdew-Burke-Ernzerhof functionals revised for solids (PBEsol) was adopted to get reliable exchange and correlation of electrons [25]. Valence electrons of $5p^6 5d^1 6s^2$, $4s^2 4p^1$, $3d^6 4s^2$, and $2s^2 2p^4$ were considered for Lu, Ga, Fe, and O, respectively. The localized Fe $3d$ electrons were treated with an effective Hubbard $U_{\text{eff}} = U - J = 4.0$ eV, which was also adopted in Refs. [9,18,26–28] for iron oxides, and such U_{eff} yields a magnetic moment of $\sim 4 \mu_B$ on Fe, being in quantitative agreement with calculations employing hybrid functionals [9], and yields band gaps of $\text{Lu}(\text{Ga})\text{FeO}_3$ in the $Pnma$, $P6_3cm$, and $Pna2_1$ phases being 2.3, 1.3, and 2.23 eV, respectively, which also agree with previous theoretical calculations (2.0, 1.3–1.4, and 2.2 eV, respectively) [18,22,29–31].

The lattice constants and atomic positions were optimized until the Hellmann-Feynman forces were less than 0.001 eV/Å. The Brillouin zone was sampled by $2 \times 2 \times 2$ ($Pnma$ and $P6_3cm$ phases) and $2 \times 3 \times 3$ ($Pna2_1$ phase) Γ -centered k -point grids. The electric polarization was calculated using the Berry phase method [32,33]. The calculations of density of states (DOS) and band gaps adopted the tetrahedron method and considered the SOC effect that enables possible noncollinear spins. It is important to know that, if only collinear spins were considered, the band gap of the $P6_3cm$ phase was found to be significantly underestimated.

The solid solutions of $\text{Lu}_{1-x}\text{Ga}_x\text{FeO}_3$ (with x ranging between 0 and 1) are simulated with 120-atom supercells for all three aforementioned phases, i.e., $3 \times 2 \times 1$ for $Pnma$ (that has 20 atoms per primitive cell), $2 \times 2 \times 1$ for $P6_3cm$ (that has 30 atoms per primitive cell), and $3 \times 1 \times 1$ for $Pna2_1$ (that has 40 atoms per primitive cell), in terms of their respective primitive unit cells. Note that an alternative hexagonal phase, i.e., the antipolar $P\bar{3}c1$ structure, which was proposed in Ref. [34], is not considered here, as it is numerically found to have higher energy than the polar $P6_3cm$ phase. In each supercell, there are 24 A -site atoms, which are occupied by Lu or Ga with a random distribution. In practice, we generated $24 \times x$ (rounded to the closest integer) random integers between 1 and 24 without repetition, where x is the composition of Ga in $\text{Lu}_{1-x}\text{Ga}_x\text{FeO}_3$. Then, the A sites on these randomly chosen positions are occupied by Ga, and the rest of the A -site positions are occupied by Lu. Here, only A -site substitution is considered, because (1) test calculations show that B -site substitution in the 120-atom supercell yields higher formation energy than A -site substitution, (2) GaFeO_3 has been synthesized experimentally [20–22], while to our knowledge the existence of LuGaO_3 was rarely reported, and (3) the doping

site could be managed by controlling the composition of each atomic species. Note that we numerically find that ordered distributions have higher energies than disordered ones. For each composition, a few disordered configurations are considered, and the one with the lowest energy is used, as it is statistically most probable to occur. Also note that calculated formation energies of $\text{Lu}_{1-x}\text{Ga}_x\text{FeO}_3$ solid solution upon decomposition into $Pnma$ LuFeO_3 and $Pna2_1$ GaFeO_3 indicate that this is an immiscible binary alloy system, however, we focus on 0-K properties and therefore temperature effects that can stabilize the solid solution phase are not considered here.

The magnetic configurations of the $Pnma$, $P6_3cm$, and $Pna2_1$ phases are G -type AFM (G -AFM), 120° noncollinear magnetic order (denoted as Y -AFM), and AFM, respectively, as consistent with previous studies [9,18,29]. Other magnetic orderings, such as ferromagnetism, A -type AFM, and C -type AFM are numerically found to yield higher energies. To allow noncollinear magnetic structures, SOC was taken into account in all calculations. Note that different random Ga distribution of the same composition may slightly affect the energetics, but test calculations on $\text{Lu}_{0.5}\text{Ga}_{0.5}\text{FeO}_3$ indicate that this effect is apparently much less than the energy change when varying Ga composition. We also note that Ga substitution may result in a slightly different magnetic ground state in the hexagonal phase, such as another Y -AFM configuration with rotated magnetic moments. These magnetic phases can be regarded as similar and their very small energy differences [9] would not affect the structural transitions.

III. RESULTS

A. Crystal and magnetic structures

Crystal structures of the $Pnma$, $P6_3cm$, and $Pna2_1$ phases are shown in Fig. 1. The $Pnma$ phase [Fig. 1(a)] belongs to the perovskite family, which has octahedrally coordinated Fe^{3+} ions. The octahedra have antiphase in-plane tiltings and in-phase out-of-plane rotations, i.e., they adopt the $a^-a^-c^+$ pattern in Glazer's notation, and the cations have antipolar displacements along the pseudocubic [110] direction. Our DFT relaxed lattice constants of the $Pnma$ phase of pure LuFeO_3 ($a = 5.14$ Å, $b = 5.51$ Å, $c = 7.49$ Å) are in good agreement with previous theoretical values ($a = 5.15$ Å, $b = 5.48$ Å, $c = 7.47$ Å) [29].

In contrast, $P6_3cm$ and $Pna2_1$ phases are nonperovskites. The unit cell of the $P6_3cm$ phase consists of two Lu-O and Fe-O layers, and the Lu and Fe atoms form respective triangular lattice [Fig. 1(b)]. Each Fe is surrounded by five oxygen atoms (two apical and three equatorial) forming a FeO_5 trigonal bipyramid, while each Lu (or Ga) is surrounded by eight oxygen atoms. These Lu (or Ga) and FeO_5 trigonal bipyramid layers are alternately stacked along the c axis. The inversion symmetry of this lattice structure is lifted by the tiltings of the FeO_5 trigonal bipyramids, generating ferroelectricity in h - LuFeO_3 [15]. The calculated lattice constants of $P6_3cm$ LuFeO_3 ($a = b = 5.94$ Å, $c = 11.53$ Å) are consistent with previous experimental ($a = b = 5.965$ Å, $c = 11.702$ Å) [2] and theoretical values ($a = b = 5.915$ Å, $c = 11.572$ Å) [9].

Figure 1(c) shows the polar $Pna2_1$ structure, which has four different cation sublattices labeled Fe1, Fe2 and Ga1,

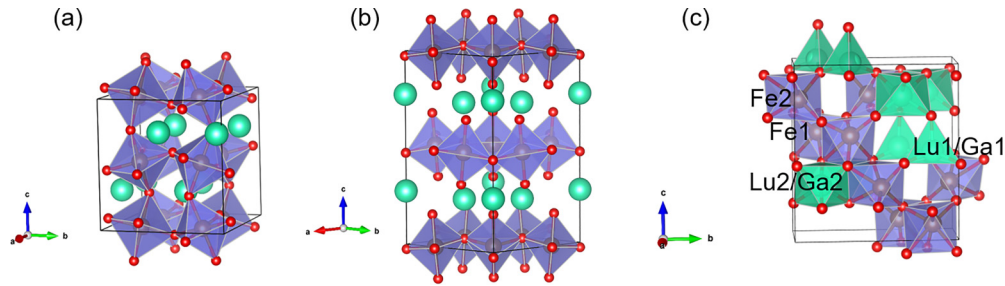


FIG. 1. The optimized crystal structures of $\text{Lu}(\text{Ga})\text{FeO}_3$. (a) The orthorhombic $Pnma$ perovskite phase with octahedrally coordinated Fe^{3+} . (b) The hexagonal $P6_3cm$ phase with FeO_5 trigonal bipyramids. (c) The orthorhombic $Pna2_1$ phase with octahedrally coordinated Fe^{3+} . The bright green, brown, and red spheres represent the $\text{Lu}(\text{Ga})$, Fe , and O atoms, respectively.

Ga2 (or occupied by Lu), respectively. The Ga2 site is surrounded by six oxygen ions forming a FeO_6 oxygen octahedron. The Ga1 site is distinctly different from Ga2 , which is surrounded by four oxygen ions, i.e., being located inside an oxygen tetrahedron. The Fe1 and Fe2 ions are in an oxygen distorted octahedral environment surrounded by six oxygen atoms. Our relaxed lattice constants of $Pna2_1$ GaFeO_3 ($a = 5.14 \text{ \AA}$, $b = 8.85 \text{ \AA}$, $c = 9.51 \text{ \AA}$) agree quite well with previous DFT calculations ($a = 5.14 \text{ \AA}$, $b = 8.82 \text{ \AA}$, $c = 9.50 \text{ \AA}$) and experimental values ($a = 5.08 \text{ \AA}$, $b = 8.74 \text{ \AA}$, $c = 9.38 \text{ \AA}$) [20,35].

The magnetic ground states for the $Pnma$, $P6_3cm$, and $Pna2_1$ phases are shown in Fig. 2. In the orthorhombic pure LuFeO_3 $Pnma$ phase, the ground state corresponds primarily to G -AFM configuration on the Fe sites with the magnetic moments aligned along the pseudocubic $[1-10]$ direction in the a - b plane, together with a small canting toward the c axis yielding a weak magnetization [Fig. 2(a)] [13,15,29,36]. The same magnetic order retains with Ga substitution, while in h - LuFeO_3 ($P6_3cm$ phase), the Γ_2 magnetic state has the lowest energy [9]. As illustrated in Fig. 2(b), the spins on the Fe sites of the same layer are aligned in the a - b plane in a 120° antiferromagnetic order named Y -AFM, and a small canting of the spins out of the a - b plane leading to a weak ferromagnetic vector further happens [9,15]. Between adjacent layers along the c axis, magnetic moments on the Fe atoms in the top layer are opposite to those in the bottom layer, indicated by red and blue arrows, respectively. Since collinear magnetic configurations are often adopted in DFT calculations, we also consider a collinear AFM structure without SOC for comparison, as shown in Fig. 2(b). Moreover, the

magnetic ground-state structure of $Pna2_1$ GaFeO_3 is known to be AFM, which originates from superexchange mediated via the Fe-O-Fe bonds [20,29] that leads to a layered magnetic ordering [Fig. 2(c)]. The magnetic moments of the Fe ions occupying the Fe1 sites are oriented in opposite directions to those of the Fe2 sites.

B. Structural evolution in $\text{Lu}_{1-x}\text{Ga}_x\text{FeO}_3$

For the above-mentioned three structures, let us first investigate the energetics in pure LuFeO_3 . Since the magnetic structures can be noncollinear, the SOC effect is taken into consideration. The obtained energies of the $Pnma$, $P6_3cm$, and $Pna2_1$ phases are -40.764 , -40.737 , and -40.329 eV per formula unit, respectively, i.e., the $Pna2_1$ phase has much higher energy, while the $Pnma$ phase has slightly lower energy than that of the $P6_3cm$ phase by 27.19 meV/f.u.; hence the $Pnma$ phase is the ground state, which is consistent with previous studies [18,37].

To explore the structural changes upon Ga substitution of Lu , we calculated the total energies of $\text{Lu}_{1-x}\text{Ga}_x\text{FeO}_3$ with increasing composition and explicit doping in a 120-atom supercell for the three candidate structures, viz., the $Pnma$, $P6_3cm$, and $Pna2_1$ phases. The magnetic structures mentioned in Sec. A are adopted as initial configurations, and note that the relative energy change due to varied magnetic orientations (such as the different arrangements in the $P6_3cm$ phase that result in $\Delta E \sim 1.2$ meV [9]) is much smaller than that due to structural changes. Therefore, the magnetic effect on the critical composition of phase transitions should be negligible. However, the energy difference between collinear and

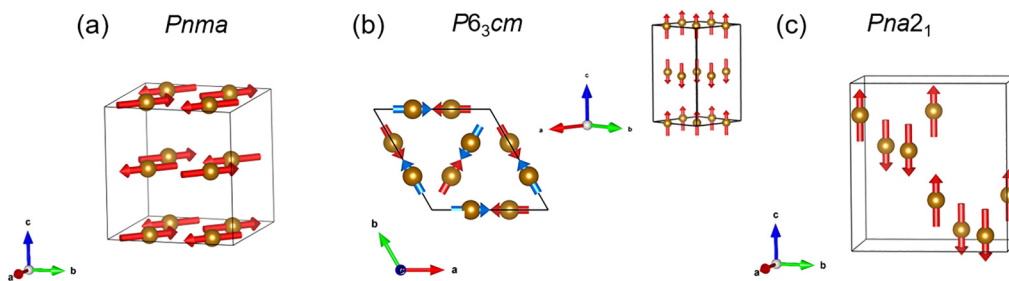


FIG. 2. Magnetic configurations in the three phases of $\text{Lu}(\text{Ga})\text{FeO}_3$: (a) G -AFM for the $Pnma$ phase; (b) top view of Y -AFM and side view of collinear AFM for the $P6_3cm$ phase; (c) AFM for the $Pna2_1$ phase. The arrows represent the directions of magnetic moments on the Fe atoms. For clarity, $\text{Lu}(\text{Ga})$ and O ions are not shown.

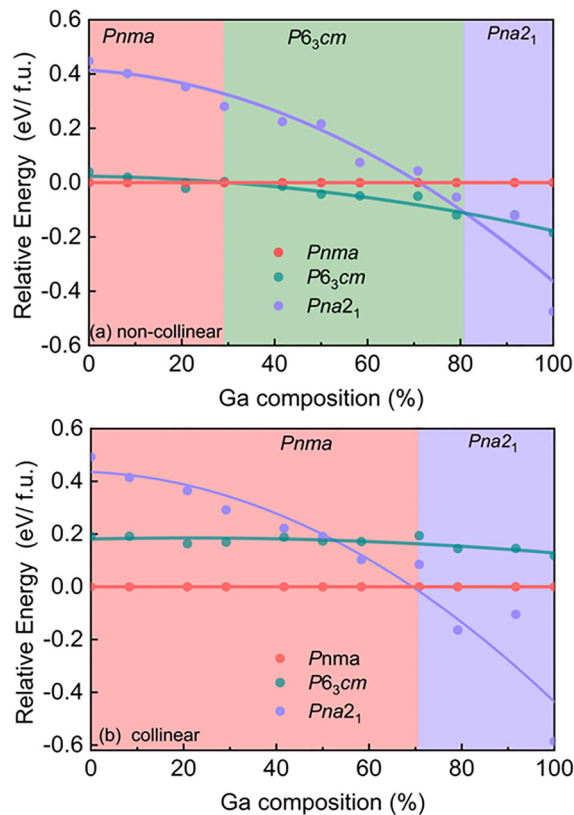


FIG. 3. DFT calculated energies of the $Pnma$, $P6_3cm$, and $Pna2_1$ phases of $\text{Lu}_{1-x}\text{Ga}_x\text{FeO}_3$ as a function of Ga composition, with the energies of the $Pnma$ phase as reference. (a) Noncollinear spins considered. (b) Collinear spins considered. The solid lines are guide to the eye from second-order polynomial fitting.

noncollinear magnetic configurations in the $P6_3cm$ phase can be significant due to the hexagonal lattice and the strong antiferromagnetic exchange coupling of the nearest planar Fe neighbors [9], which will be discussed next.

The calculated relative energies are presented in Fig. 3(a), taking the $Pnma$ phase as reference, and the following transitions are obtained. First, the nonpolar $Pnma$ state remains to be the most stable phase when the Ga concentration is below 29%. With increasing composition, both the $P6_3cm$ and $Pna2_1$ phases have decreased energies with respect to $Pnma$, albeit the stronger the decrease from the $Pna2_1$ phases, the polar $P6_3cm$ phase starts with a much lower energy and becomes the ground state in the range of $29\% < x < 81\%$. Further increasing Ga composition results in a second transition from $P6_3cm$ to $Pna2_1$ for Ga compositions above 81%.

It is worthwhile to point out that the noncollinear Y -AFM magnetic structure in the $P6_3cm$ phase is very important for the stabilization of this structure. As a matter of fact, and as shown in Fig. 3(b), if only collinear spin structures [without SOC, see Fig. 2(b) right panel] are considered in the computations, there will be only a single transition from $Pnma$ to $Pna2_1$ at 69.4%. The relative energies of the $Pnma$ and $Pna2_1$ phases are much less affected since their AFM structures are close to be collinear, whereas for the $P6_3cm$ phase the energy increases for nearly 0.2 eV/f.u. Therefore, only results with noncollinear spins (with SOC effect) will be discussed in the following.

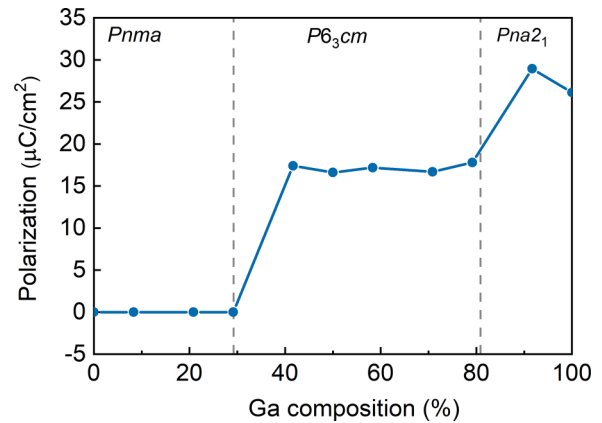


FIG. 4. DFT calculated polarization of $\text{Lu}_{1-x}\text{Ga}_x\text{FeO}_3$ as a function of Ga composition. For each composition, only the structure with the lowest energy, i.e., the ground state, is considered.

C. Multiferroic properties

Next, let us check whether Ga substitution can tune LuFeO_3 to be both ferroelectric and ferromagnetic. The change of electric polarization as a function of Ga composition is shown in Fig. 4, where only the ground state of each case is considered. One can see that, while $\text{Lu}_{1-x}\text{Ga}_x\text{FeO}_3$ is in the $Pnma$ state, i.e., when $0 < x < 29\%$, the polarization is zero. Such phase may be paraelectric or antiferroelectric, depending on if a first-order transition to a ferroelectric phase can occur upon application of a feasible electric field. With the composition being between 29% and 81%, the most stable $P6_3cm$ phase has a sizable polarization approximately of $17.4 \mu\text{C}/\text{cm}^2$ at 42% due to up-down-down displacements of Lu^{3+} (Ga^{3+}) ions, which basically saturates with further increase of x within this phase. Note that the polarization of the metastable pure h - LuFeO_3 is calculated to be $10.5 \mu\text{C}/\text{cm}^2$, being consistent with other theoretical values [9,18]. After Ga doping, the same structure thus has an increased polarization. Upon further increase of composition, the $Pna2_1$ phase becomes the ground state, which also exhibits a spontaneous polarization of about $26 \mu\text{C}/\text{cm}^2$, being in agreement with

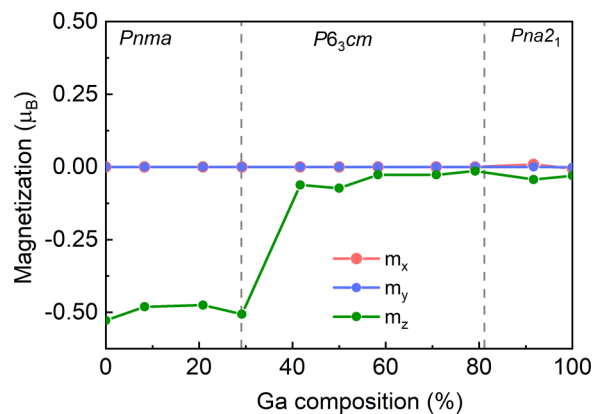


FIG. 5. DFT calculated weak magnetization of $\text{Lu}_{1-x}\text{Ga}_x\text{FeO}_3$ (120-atom supercell) as a function of Ga composition. For each composition, only the structure with the lowest energy, i.e., the ground state, is considered.

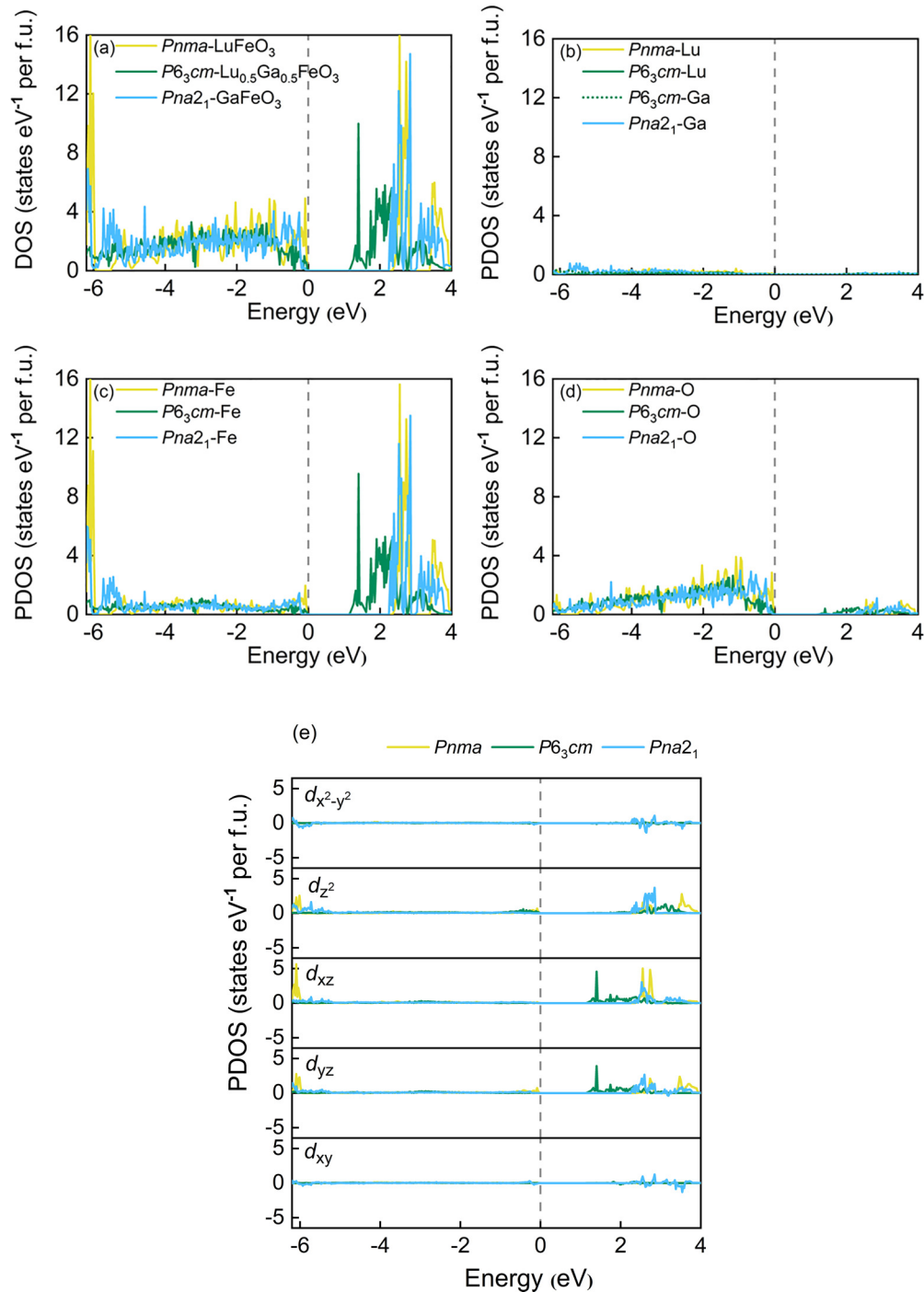


FIG. 6. DFT calculated density of states of LuFeO₃, Lu_{0.5}Ga_{0.5}FeO₃, and GaFeO₃ in the *Pnma*, *P6₃cm*, and *Pna2₁* phase, respectively. (a) Total DOS. (b) Partial DOS for Lu/Ga. (c) Partial DOS for Fe. (d) Partial DOS for O. (e) Orbital resolved partial DOS for Fe. The zero energy is set as the top of the valence band.

reported experimental and theoretical data [22] and slightly larger than that of the *P6₃cm* phase.

While Lu_{1-x}Ga_xFeO₃ undergoes the *Pnma* → *P6₃cm* → *Pna2₁* phase transitions, the magnetic structure changes accordingly in the sequence of *G*-AFM, *Y*-AFM, and AFM, all with canted weak magnetization being allowed in our calculations. Figure 5 reports the calculated ferromagnetic moment as a function of composition for the stable structures.

Similar to pure *Pnma* LuFeO₃, the spins on the Fe sites of the *Pnma* Lu_{1-x}Ga_xFeO₃ ($x = 0.0 - 0.29$) order antiferromagnetically along the [1-10] direction; a canting towards the *z*-axis generates a weak ferromagnetism. As presented in Fig. 5, when Lu_{1-x}Ga_xFeO₃ is in the *Pnma* state, the magnetization along the *x* and *y* directions are both zero while the magnetization along the *z* direction basically remains to be around $-0.5 \mu_B$. For pure *h*-LuFeO₃ of the 120-atom

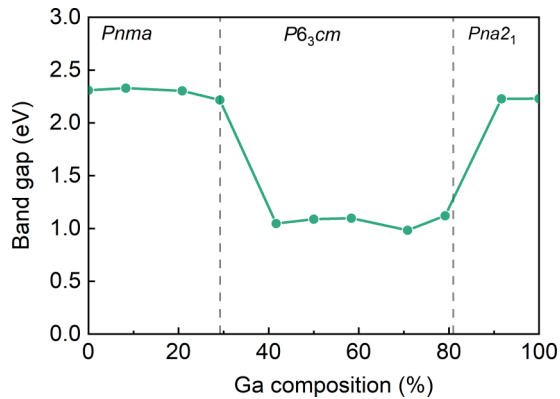


FIG. 7. DFT calculated band gap of $\text{Lu}_{1-x}\text{Ga}_x\text{FeO}_3$ as a function of Ga composition. For each composition, only the structure with the lowest energy, i.e., the ground state, is considered.

supercell, there is only a weak magnetization along the z direction with zero in-plane component, and it is about $-0.15 \mu_B$. For 120-atom supercell $h\text{-Lu}_{1-x}\text{Ga}_x\text{FeO}_3$, however, due to the irregular positions of Ga atoms that break the hexagonal symmetry, small m_x and m_y can occur. Since this is a computational limitation that the in-plane components should vanish in real samples or very large supercells if averaged over sufficient number of random distributions, m_x and m_y are reported to be zero in Fig. 5. m_z in $P6_3cm$ $\text{Lu}_{1-x}\text{Ga}_x\text{FeO}_3$ at $x = 0.42$ ($-0.06 \mu_B$) is smaller than the value in pure $h\text{-LuFeO}_3$ ($-0.15 \mu_B$) [10,12,38]. Such weak magnetization slowly decreases with increasing Ga doping until $x = 0.81$. When $\text{Lu}_{1-x}\text{Ga}_x\text{FeO}_3$ is in the $Pna2_1$ phase ($x = 0.81 - 1.0$), the magnetization is essentially close to zero, as was also reported in Ref. [20] for pure GaFeO_3 .

D. Electronic properties

The electronic properties also evolve with the structural phase transitions, as indicated by the variations of DOS and band gaps. As representative examples, the DOS of pure LuFeO_3 of $Pnma$ phase, $\text{Lu}_{0.5}\text{Ga}_{0.5}\text{FeO}_3$ of the $P6_3cm$ phase and GaFeO_3 of the $Pna2_1$ phase are shown in Fig. 6. The total DOS [Fig. 6(a)] shows similarity of the valence band for the three phases, but the conduction band minimum is significantly reduced in the $P6_3cm$ phase as compared to the other two structures, which very much resemble each other. Specifically, the valence band maximum is contributed mostly by O and slightly by Fe [Figs. 6(b), 6(c), and 6(d)], while the conduction band minimum is dominated by the Fe d_{xy} orbital, as illustrated by the partial DOS of Fe in Fig. 6(e).

The variation of the band gap E_g of $\text{Lu}_{1-x}\text{Ga}_x\text{FeO}_3$ is reported in Fig. 7, as determined by the separation between valence band maximum and conduction band minimum from the DOS calculations. With all phases being semiconductors, the band gaps of LuFeO_3 , $\text{Lu}_{0.5}\text{Ga}_{0.5}\text{FeO}_3$, and GaFeO_3 in respectively the $Pnma$, $P6_3cm$, and $Pna2_1$ phases are 2.3, 1.09, and 2.23 eV. The values of pure LuFeO_3 ($Pnma$ phase) and pure GaFeO_3 ($Pna2_1$ phase) are in good agreement with

previous theoretical calculations (2.0 and 2.2 eV, respectively) [22,29,30]. The computed band gap of pure $h\text{-LuFeO}_3$ is 1.30 eV, which is also consistent with reported theoretical values of 1.3–1.4 eV [18,31], and $h\text{-Lu}_{0.5}\text{Ga}_{0.5}\text{FeO}_3$ has a similar value of $E_g = 1.09$ eV, suggesting that the electronic structure around the Fermi level is rather insensitive to Ga doping, since the Lu (or Ga) bands are not significant in this energy range [see Fig. 6(b)].

Therefore, interestingly, the band gap is mainly determined by the overall structure, i.e., E_g is around 2.3 eV when $\text{Lu}_{1-x}\text{Ga}_x\text{FeO}_3$ is in the $Pnma$ phase ($0 < x < 29\%$); E_g decreases abruptly in the $P6_3cm$ phase to about 1.0 eV; and E_g recovers abruptly to 2.23 eV in the $Pna2_1$ phase. Therefore, this further indicates that different Ga compositions cause changes in the structure of $\text{Lu}_{1-x}\text{Ga}_x\text{FeO}_3$ and then different structural states lead to different values of E_g . In addition, when $\text{Lu}_{1-x}\text{Ga}_x\text{FeO}_3$ is in the same phase, the values of E_g are basically very close to each other and do not change significantly, nearly irrespective of the Ga composition.

IV. CONCLUSIONS

In summary, we have investigated bulk $\text{Lu}_{1-x}\text{Ga}_x\text{FeO}_3$ for its structural phase transitions as a function of Ga composition and its multiferroic properties, using *ab initio* calculations. We find that $\text{Lu}_{1-x}\text{Ga}_x\text{FeO}_3$ undergoes the transitions of $Pnma$ ($x = 0 - 0.29$) \rightarrow $P6_3cm$ ($x = 0.29 - 0.81$) \rightarrow $Pna2_1$ ($x = 0.81 - 1$) by varying the concentration of Ga. Associated with such transitions, the electric polarization changes from zero in the nonpolar $Pnma$ phase to $17 \mu\text{C}/\text{cm}^2$ in the $P6_3cm$ phase, and then to as large as $29 \mu\text{C}/\text{cm}^2$ in the $Pna2_1$ phase; meanwhile, the magnetization decreases from $-0.5 \mu_B$ ($Pnma$) to $-0.06 \mu_B$ ($P6_3cm$) and nearly zero ($Pna2_1$). Within each phase, the polarization and magnetization are found to be rather insensitive to Ga composition. The $P6_3cm$ phase is both ferroelectric and weakly ferromagnetic. The electronic band gaps are also found to vary with the phase transitions, with a significant drop from about 2.3 eV in the $Pnma$ and $Pna2_1$ phases to 1.09 eV in the $P6_3cm$ phase. Therefore, we believe that Ga substitution is an effective means to tune the multiferroic, electronic, and optical properties of LuFeO_3 and hope that our findings can be verified by future experiments.

ACKNOWLEDGMENTS

We thank H. J. Zhao, C. S. Xu, and C. Liu for helpful discussions. This work was supported by National Natural Science Foundation of China (Grant No. 12074277), the startup fund from Soochow University, and the support from Priority Academic Program Development (PAPD) of Jiangsu Higher Education Institutions. L.B. thanks the Office of Naval Research (Grant No. N00014-21-1-2086) and Vannevar Bush Faculty Fellowship (VBFF) Grant No. N00014-20-1-2834 from the Department of Defense. The authors also acknowledge the High-Performance Computer Center (HPCC) resources of Arkansas University and HPCC of Nantong University for the computations.

- [1] S.-W. Cheong and M. Mostovoy, *Nat. Mater.* **6**, 13 (2007).
- [2] E. Magome, C. Moriyoshi, Y. Kuroiwa, A. Masuno, and H. Inoue, *Jpn. J. Appl. Phys.* **49**, 09ME06 (2010).
- [3] J. F. Scott, *Nat. Mater.* **6**, 256 (2007).
- [4] S. Dong, J.-M. Liu, S.-W. Cheong, and Z. Ren, *Adv. Phys.* **64**, 519 (2015).
- [5] Y. K. Jeong, J.-H. Lee, S.-J. Ahn, and H. M. Jang, *Chem. Mater.* **24**, 2426 (2012).
- [6] W. Wang, J. Zhao, W. Wang, Z. Gai, N. Balke, M. Chi, H. N. Lee, W. Tian, L. Zhu, X. Cheng, D. J. Keavney, J. Yi, T. Z. Ward, P. C. Snijders, H. M. Christen, W. Wu, J. Shen, and X. Xu, *Phys. Rev. Lett.* **110**, 237601 (2013).
- [7] A. A. Bossak, I. E. Graboy, O. Y. Gorbenko, A. R. Kaul, M. S. Kartavtseva, V. L. Svetchnikov, and H. W. Zandbergen, *Chem. Mater.* **16**, 1751 (2004).
- [8] H. W. Wang, I. V. Solovyev, W. B. Wang, X. Wang, P. J. Ryan, D. J. Keavney, J. W. Kim, T. Z. Ward, L. Y. Zhu, J. Shen, X. M. Cheng, L. X. He, X. S. Xu, and X. F. Wu, *Phys. Rev. B* **90**, 014436 (2014).
- [9] C. Xu, Y. Yang, S. Wang, W. Duan, B. Gu, and L. Bellaiche, *Phys. Rev. B* **89**, 205122 (2014).
- [10] A. R. Akbashev, A. S. Semisalova, N. S. Perov, and A. R. Kaul, *Appl. Phys. Lett.* **99**, 122502 (2011).
- [11] J. A. Moyer, R. Misra, J. A. Mundy, C. M. Brooks, J. T. Heron, D. A. Muller, D. G. Schlom, and P. Schiffer, *APL Mater.* **2**, 012106 (2014).
- [12] S. M. Disseler, J. A. Borchers, C. M. Brooks, J. A. Mundy, J. A. Moyer, D. A. Hillsberry, E. L. Thies, D. A. Tenne, J. Heron, M. E. Holtz, J. D. Clarkson, G. M. Stiehl, P. Schiffer, D. A. Muller, D. G. Schlom, and W. D. Ratcliff, *Phys. Rev. Lett.* **114**, 217602 (2015).
- [13] R. L. White, *J. Appl. Phys.* **40**, 1061 (1969).
- [14] X. Xu and W. Wang, *Mod. Phys. Lett. B* **28**, 1430008 (2014).
- [15] S. Cao, X. Zhang, T. R. Paudel, K. Sinha, X. Wang, X. Jiang, W. Wang, S. Brutsche, J. Wang, P. J. Ryan, J.-W. Kim, X. Cheng, E. Y. Tsybmal, P. A. Dowben, and X. Xu, *J. Phys.: Condens. Matter* **28**, 156001 (2016).
- [16] S. M. Disseler, X. Luo, B. Gao, Y. S. Oh, R. W. Hu, Y. Z. Wang, D. Quintana, A. Zhang, Q. Z. Huang, J. Lau, R. Paul, J. W. Lynn, S.-W. Cheong, and W. Ratcliff, II, *Phys. Rev. B* **92**, 054435 (2015).
- [17] A. Masuno, A. Ishimoto, C. Moriyoshi, N. Hayashi, H. Kawaji, Y. Kuroiwa, and H. Inoue, *Inorg. Chem.* **52**, 11889 (2013).
- [18] L. Lin, H. M. Zhang, M. F. Liu, Shoudong Shen, S. Zhou, D. Li, X. Wang, Z. B. Yan, Z. D. Zhang, Jun Zhao, Shuai Dong, and J.-M. Liu, *Phys. Rev. B* **93**, 075146 (2016).
- [19] J. Liu, T. L. Sun, X. Q. Liu, H. Tian, T. T. Gao, and X. M. Chen, *Adv. Funct. Mater.* **28**, 1706062 (2018).
- [20] J. Atanelov and P. Mohn, *Phys. Rev. B* **92**, 104408 (2015).
- [21] S. Song, H. M. Jang, N.-S. Lee, J. Y. Son, R. Gupta, A. Garg, J. Ratanapreechachai, and J. F. Scott, *NPG Asia Mater.* **8**, e242 (2016).
- [22] D. Stoeffler, *J. Phys.: Condens. Matter* **24**, 185502 (2012).
- [23] G. Kresse and J. Hafner, *Phys. Rev. B* **47**, 558 (1993).
- [24] G. Kresse and J. Furthmüller, *Phys. Rev. B* **54**, 11169 (1996).
- [25] J. P. Perdew, A. Ruzsinszky, G. I. Csonka, O. A. Vydrov, G. E. Scuseria, L. A. Constantin, X. L. Zhou, and K. Burke, *Phys. Rev. Lett.* **100**, 136406 (2008).
- [26] S. L. Dudarev, G. A. Botton, S. Y. Savrasov, C. J. Humphreys, and A. P. Sutton, *Phys. Rev. B* **57**, 1505 (1998).
- [27] J. B. Neaton, C. Ederer, U. V. Waghmare, N. A. Spaldin, and K. M. Rabe, *Phys. Rev. B* **71**, 014113 (2005).
- [28] R. Nakamoto, B. Xu, C. Xu, H. Xu, and L. Bellaiche, *Phys. Rev. B* **95**, 024434 (2017).
- [29] U. Chowdhury, S. Goswami, A. Roy, S. Rajput, A. K. Mall, R. Gupta, S. D. Kaushik, V. Siruguri, S. Saravanakumar, S. Israel, R. Saravanan, A. Senyshyn, T. Chatterji, J. F. Scott, A. Garg, and D. Bhattacharya, *Phys. Rev. B* **100**, 195116 (2019).
- [30] Z. H. Sun, S. Dai, Y. L. Zhou, L. Z. Cao, and Z. H. Chen, *Thin Solid Films* **516**, 7433 (2008).
- [31] W. B. Wang, H. W. Wang, X. Y. Xu, L. Y. Zhu, L. X. He, E. Wills, X. M. Cheng, D. J. Keavney, J. Shen, X. F. Wu, and X. S. Xu, *Appl. Phys. Lett.* **101**, 241907 (2012).
- [32] R. D. King-Smith and D. Vanderbilt, *Phys. Rev. B* **47**, 1651 (1993).
- [33] R. Resta, *Rev. Mod. Phys.* **66**, 899 (1994).
- [34] J. Nordlander, M. A. Anderson, C. M. Brooks, M. E. Holtz, and J. A. Mundy, *Appl. Phys. Rev.* **9**, 031309 (2022).
- [35] M. Hatnean, J. Robert, M. T. Fernandez Diaz, E. Ressouche, A. Cousson, L. Pinsard-Gaudart, and S. Petit, *Eur. Phys. J. Spec. Top.* **213**, 69 (2012).
- [36] M. Iglesias, A. Rodríguez, P. Blaha, V. Pardo, D. Baldomir, M. Pereiro, J. Botana, J. E. Arias, and K. Schwarz, *J. Magn. Magn. Mater.* **290-291**, 396 (2005).
- [37] W. Zhu, L. Pi, S. Tan, and Y. Zhang, *Appl. Phys. Lett.* **100**, 052407, (2012).
- [38] A. T. Melo, D. M. S. Brito, A. F. Lima, and M. V. Lalic, *J. Alloys Compd.* **813**, 152227 (2020).